

The Dynamical Implications of Multiple Stellar Formation Events in Galactic Globular Clusters

Jonathan M.B. Downing¹ and Alison Sills

*Department of Physics and Astronomy, ABB-241, McMaster University, 1280 Main Street
West, Hamilton, Ontario, L8S 4M1, Canada*

downin@ari.uni-heidelberg.de, asills@mcmaster.ca

ABSTRACT

Various galactic globular clusters display abundance anomalies that affect the morphology of their colour-magnitude diagrams. In this paper we consider the possibility of helium enhancement in the anomalous horizontal branch of NGC 2808. We examine the dynamics of a self-enrichment scenario in which an initial generation of stars with a top-heavy initial mass function enriches the interstellar medium with helium via the low-velocity ejecta of its asymptotic giant branch stars. This enriched medium then produces a second generation of stars which are themselves helium-enriched. We use a direct N-body approach to perform five simulations and conclude that such two-generation clusters are both possible and would not differ significantly from their single-generation counterparts on the basis of dynamics. We find, however, that the stellar populations of such clusters would differ from single-generation clusters with a standard initial mass function and in particular would be enhanced in white dwarf stars. We conclude, at least from the standpoint of dynamics, that two-generation globular clusters are feasible.

Subject headings: stellar dynamics — methods: N-body simulations — globular clusters: general — globular clusters: self-enrichment — globular clusters: individual(NGC 2808) — stars: AGB — stars: HB

1. Introduction

Globular clusters are gravitationally bound collections of stars, typically including between 10^3 and 10^7 members, which normally occur within the halos of galaxies. Galactic

¹Current Address: Astronomisches Rechen-Institut, Zentrum für Astronomie Universität Heidelberg, Mönchhofstraße 12-14, D-69120, Heidelberg, Germany

globular clusters are understood to be old objects, up to 12 Gyr in age (Meissner & Weiss 2006), and are thus primordial components of the galaxy. In the simple picture, all stars within a globular cluster are thought to have formed at the same time and out of the same medium, thus sharing the same age and chemical composition. In particular all stars in a given globular cluster have the same value of $[Fe/H]$ and are said to be mono-metallic. The only differentiation between stars in this scenario is their spectrum of masses determined by an initial mass function (IMF). There is thought to be a universal IMF for all galactic globular clusters but there is some debate as to its exact form (Kroupa (2002) and references therein).

Although this description works well for the most part, several globular clusters display population characteristics that are inconsistent with this model. In many clusters all stars have the same $[Fe/H]$ but there are star-to-star abundances variations in other elements. In particular many globular clusters stars show strong star-to star O-Na and Mg-Al anticorrelations (Gratton et al. 2004). Some clusters also display peculiar morphologies in the horizontal branch of the Colour-Magnitude Diagram (CMD). In some cases different clusters with the same $[Fe/H]$ and with otherwise identical colour-magnitude diagrams will have differing horizontal branch morphologies (e.g. the case of M3 and M13 (Catelan & de Freitas Pacheco (1995), Kraft et al. (1992)). This is called the “second parameter problem” since such clusters seem to require a second parameter (other than metallicity) in order to explain the variations between them. In some cases, the presence of very extended horizontal branch blue tails is linked to dynamical or abundance effects. One possible source of these anomalies is a self-enrichment scenario where chemicals produced by some cluster stars are incorporated into other cluster stars which then display unusual characteristics such as enhancements of light and heavy elements (particularly products of hot-hydrogen burning and the CNO cycle) and unusual colours (frequently bluer) with respect to field stars (see the review by Gratton et al. (2004) for further details). We propose to explore the dynamics of a particular variation of the self-enrichment scenario in which excess helium is produced by asymptotic giant branch (AGB) stars and which may generate the anomalous horizontal branch of the globular cluster NGC 2808.

NGC 2808 is a southern galactic globular cluster first observed in detail in the late 1960s (Alcaino 1969). It is quite massive at $1.6 \times 10^6 M_{\odot}$, has a moderately high velocity dispersion $\sigma_o = 13.4 km/s$ (Pryor & Meylan 1993) and is relatively metal rich with $[Fe/H] = -1.09$ (Harris 1996). As early as 1974 a peculiar morphology (both bimodal and extended) was discovered in the horizontal branch (HB) of the CMD of NGC 2808 (Harris 1974). The horizontal branch of NGC 2808 consists of both a small horizontal clump (hereafter called the red horizontal branch or RHB) and a separate, extended tail reaching vertically from 16th to 22nd magnitude (hereafter called the blue horizontal branch or BHB). The BHB

is also multi-modal with three distinct groups (called from top to bottom extended blue tails (EBTs) 1, 2 and 3). This is very different from canonical HB morphology (flat and monomodal) and in order to explain it a special scenario is required.

One way to explain the anomalous morphology of the HB of NGC 2808 is to assume that the BHB stars are helium enriched while the RHB stars contain the cosmological helium abundance of $Y \sim 0.24$ (D’Antona et al. 2002). The enrichment cannot be attributed to helium variations across the primordial cloud since the necessary levels of enrichment are extreme ($Y \sim 0.32 - 0.4$ is needed in EBT 3 (D’Antona & Caloi 2004), (D’Antona et al. 2005)) and the helium must arise from stellar processes through self-enrichment. It has been argued (Gnedin et al. 2002) that the more massive globular clusters (particularly ω -Centari) may have sufficient self-gravity to retain the low-velocity ejecta from AGB stars (and in the case of the most massive even some of the ejecta from Type II supernova). In the case of clusters within ~ 10 kpc (such as ω -Centari) Gnedin et al. (2002) argue that interaction with the galactic disc would strip such ejecta from clusters before it can experience star formation. NGC 2808, however, is 11.1 kpc from the galactic center (Harris 1996) and may avoid such stripping long enough to undergo a second generation of star formation (D’Antona & Caloi 2004). This leads to a scenario in which helium self-enrichment from AGB stars produces the horizontal branch morphology of NGC 2808. In particular D’Antona & Caloi (2004) propose a model where NGC 2808 has experienced two stellar formation events. The first event features a top-heavy mass function that enhances the number of $3 - 5 M_{\odot}$ stars. These evolve to the asymptotic giant branch (AGB) phase in ≤ 200 Myr and enrich the interstellar medium (ISM) with helium (and other elements) through stellar winds. A second generation of stars then forms from the helium-enriched ISM. An age difference of ≤ 200 Myr would not be observable because it is a small fraction of the lifetime of a low mass star, but the helium difference in the populations would be. The low-mass stars in the first generation would form the RHB of NGC 2808 and the enriched second generation would form the BHB. The multi-modality of the BHB (EBTs 1, 2 and 3) can be explained by varying levels of helium enrichment produced either by several minor stellar formation events producing different levels of helium enrichment or possibly by differential helium enrichment across the cluster. Modeling more than two generations or trying to account for spatially dependent helium enhancement is beyond the scope of our simulations and in this paper we do not investigate the substructure in the BHB. It is possible that helium enrichment is the source of other anomalous CMD morphologies. Notably the double main sequence of the massive cluster ω Centauri can be explained if the blue main sequence stars are helium enriched (Piotto et al. 2005)¹. Indeed D’Antona et al. (2005) claim helium enrichment in some 20%

¹ ω Centauri has many other peculiarities and may be the core of a stripped dwarf galaxy. It cannot be

of main sequence stars for NGC 2808 (although this case is less clear cut) but we have not tried to model this effect.

Based on stellar evolution models D’Antona & Caloi (2004) claim that, given certain assumptions, sufficient helium can be produced by AGB stars in the two-generation scenario to explain the BHB of NGC 2808. If enhancements in other elements produced by AGB stars are ignored and the top-heavy mass function is accepted, the scenario may be plausible on the basis of stellar chemistry. The massive first generation may, however, have effects on both the dynamics and population of the cluster. Specifically the high mass of the initial generation and the effect of adding a second generation to a dynamically evolved object could lead to dynamical instabilities or affect the final spatial distribution of a star cluster. In addition the first generation will leave many intermediate-mass remnants, primarily white dwarfs, which should still be observable after 10-12 Gyr (e.g. Hansen et al. (2002)). We use a direct N-body approach to explore the dynamical evolution of a globular cluster in the D’Antona and Caloi two-generation formation scenario.

2. Method

To perform our simulations we use Starlab, a direct N-body evolution code. Starlab uses a fourth-order Hermite predictor-corrector scheme (McMillan 1986) and contains a full suite of stellar and binary evolution algorithms based on the work of Eggleton et al. (1989). Starlab is described in some detail in Portegies Zwart et al. (2001) and is freely available with some documentation from <http://www.ids.ias.edu/~starlab/>. We also use a GRAPE-6A N-body gravitational accelerator (Fukushige et al. 2005) to improve the speed and size of our simulations.

2.1. Top-Heavy IMF

The D’Antona and Caloi top-heavy IMF given in D’Antona & Caloi (2004) is a broken power-law which takes the form:

$$\frac{dN}{dM} = \begin{cases} c_1 M^{-(1+\alpha)} & \text{if } M \leq M_B \\ c_2 M^{-(1+\beta)} & \text{if } M > M_B \end{cases}$$

and is defined by the exponents α and β and a transition mass M_B (c_1 and c_2 are normalization constants). The explicit implementation of this IMF in Starlab is discussed in Appendix

considered typical of galactic globular clusters

A. A D’Antona and Caloi IMF created with this implementation where $\alpha = -0.5$, $\beta = 3.0$ and $M_B = 3.8$ is compared with a standard Salpeter IMF in Figure 1. These parameters correspond to the IMF from D’Antona & Caloi (2004) with the lowest overall mass still capable of providing the requisite helium enhancement. This is ostensibly the least extreme scenario and, since discrepancies between simulations of single-generation clusters and more extreme examples of the D’Antona and Caloi scenario might not preclude agreement in less extreme cases, we use these parameters in all of our simulations.

2.2. Details of the First Generation

In modeling the first generation there are three components to consider, one stellar and two gaseous. The stellar component is simply the stars of the first generation and can be dealt with by standard N-body modeling. The first gas component consists of the remnant gas from the first generation of star formation. The second gas component is composed of the ejecta from the AGB stars of the first generation which produces the helium enhancement for the second generation.

There is little information available on the configuration of remnant gas (first component) in young globular clusters and for simplicity we model the remnant ISM left over from the first generation of star formation as an analytic Plummer potential, $\phi(r) = -\frac{GM}{\sqrt{r^2+a^2}}$. This potential is not static since the remnant ISM is stripped from the young cluster by the radiation from young O stars, early supernovae and possibly due to interactions with the galactic disk. The exact rate of gas stripping from young clusters is unknown but it is on the order of 10s of Myrs (Goodwin (1997), Bastian & Goodwin (2006)). It is clear, however, that this mass-loss affects early cluster evolution since the potential in which the cluster lives becomes more shallow over time and the cluster can expand and in the extreme case be completely disrupted.

The stellar ejecta forming the second component originates primarily from supernovae and the stellar winds of AGB stars. According to Gnedin et al. (2002) the characteristic terminal velocity for AGB winds is $\sim 15 \text{ km s}^{-1}$ whereas the escape velocity for a cluster of the mass of NGC 2808 is on the order of 60 km s^{-1} in the core and 40 km s^{-1} at the half mass radius. It is plausible that a large fraction of the mass lost by AGB stars will in fact be retained as gas by the cluster. In our models we assume that all of the mass lost due to stellar evolution is retained, that is, we do not treat ejecta from different progenitor stars separately. This assumption is not necessarily realistic since the high-velocity supernovae ejecta may be able to escape from the potential well of the young cluster and some of the AGB ejecta may be stripped by radiation in the same way as the remnant ISM. The majority of stars

in the first generation are below $10M_{\odot}$ and will not undergo supernovae events in the first 200 Myr of the cluster’s life. Therefore the AGB ejecta should be the dominant component and including the supernovae ejecta is not a concern. The stripping fraction for the AGB ejecta is also not clear and treating it would vastly expand our parameter space without providing any particular physical insight. Thus the choice of a 100% retention fraction for the ejecta is a reasonable first approximation and is also in the spirit of D’Antona & Caloi (2004). We model the retained ejecta as another single, global Plummer potential with a mass increasing at the rate mass is lost from the stars due to stellar evolution. To be more realistic, we should add gas to the simulation locally where it is lost by the stars. Since at 15km s^{-1} the gas crossing time at the initial viral radius is ~ 3 Myr (about two simulation time units) and the particle crossing time is ~ 8.5 Myr (about four simulation time units) we expect gas produced locally to be quickly distributed throughout the cluster. Thus the assumption of a global profile for the second gas component seems reasonable.

Since Starlab does not contain prescriptions for time-evolving potentials and to incorporate such prescriptions linked both to radiation pressure and stellar evolution would be time-consuming we make the following approximations: (1) We assume that after 200 Myr all of the remnant ISM has been removed from the cluster. (2) We assume that the remnant ISM is stripped from the cluster at the same rate at which ejecta from the first generation stars is added to the cluster. (3) We assume that the initial mass of the first component is the same as the final mass of the second component. This leads to a model where the first-generation is embedded in a *static* Plummer potential with a total mass equal to the mass lost by stellar evolution in the first generation. Assumption (1) is almost certainly secure since young clusters appear to be stripped of their remnant star forming material on timescales of a few 10s of Megayears but this means assumption (2) is not necessarily accurate since the remnant ISM will be ejected more rapidly than it is replaced by the ejecta from the first generation (added to the cluster over a timescale of 200 Myr). We argue that the two interacting potentials will act in three phases. Initially the remnant ISM potential will provide a deep well which will cause the cluster to contract. Once the remnant ISM has been removed and before the ejecta potential becomes large the cluster will be able to expand normally due to mass-loss. Finally the ejecta potential will dominate and strongly mitigate the effect of mass-loss and again slow the expansion. The global static potential will have the correct behaviour at the beginning and end and will simply slightly deepen the potential in the middle phase. In both cases the dynamical effect should simply be to suppress the expansion of the cluster due to stellar-evolution mass-loss. Assumption (3) is simply convenient and, since the exact star formation rate in young clusters is unknown, any variation of this parameter would not provide any new physical insight. To confirm the static potential has no additional dynamical effects, we compare the evolution of one of our

first generations with and without a potential in Figure 2.

As expected the only qualitative difference between the two plots in Figure 2 is that with the addition of the Plummer potential both the massive and overall Lagrangian radii increase more slowly and lead to a smaller, more compact final cluster. This effect is seen in both the massive and overall Lagrangian radii and is a good indication that mass segregation has not been suppressed by the addition of the external field. Since mass-segregation is a two-body relaxation effect (Farouki & Salpeter 1982) this shows that two-body relaxation also has not been affected by the addition of the Plummer potential.

Obviously a pair of time-evolving potentials linked to the stellar physics of the code would be preferable but the difference would be in details rather than in overall effect. Any galactic globular cluster will have experienced ~ 10 Gyr of dynamical evolution since the potential formation of a second generation and thus be a fully dynamically relaxed object. Since dynamically relaxed N-body systems are insensitive to their initial conditions (Binney & Tremaine 1987) we would not expect fine details of the gas potential in the first generation to be significant for current observations. We note that our predictions are not applicable to two-generation clusters in the process of forming their second generation or even those less than a relaxation time old. For such objects, however, it is not clear that global potentials would be sufficient to accurately resolve the details of evolution and such models may have to wait until hybrid SPH-N-body codes are available.

2.3. The Second Generation

In order to match current observations we assume the second generation forms with a more standard IMF and for simplicity we choose a Salpeter IMF (Salpeter 1955). In order to implement the second generation we must find some way add stars to the output file from the simulation of the first generation (in Starlab such a file is known as a snapshot). The easiest way to implement this in Starlab is to create a separate snapshot using the parameters characterizing the second generation and then combining this snapshot with the output snapshot from the first generation using the routine `merge_snaps`. We choose the total mass of the second-generation to match the mass of the Plummer potential and hence the mass lost in our first-generation. This implicitly implies 100% star formation efficiency. This assumption is almost certainly unrealistic (e.g. Lada & Lada (2003)) but it is both in keeping with the spirit of the scenario proposed by D’Antona & Caloi (2004) and it allows us to conserve mass when adding the second generation (all of the Plummer potential mass is replaced by stellar mass). Since the actual star formation efficiency during galactic globular cluster formation is not known, considering different star formation rates

would again increase our parameter space without providing any particular physical insight. We use the `merge_snaps` routine to combine the first and second generation snapshots into a single snapshot and manually remove the Plummer potential from the first generation. This procedure represents the conversion of a continuous gas potential into a generation of stars with the same total mass in one timestep (~ 1.5 Myr). Once the second generation has been added and the Plummer potential removed, the combined cluster is evolved for ~ 12 Gyr which corresponds to 15-16 initial half-mass relaxation times (T_{RH}) (Spitzer 1987). In order to produce simulations lasting more than 2-4 initial half-mass relaxation times it is necessary to introduce a stripping radius. This is because newly-formed neutron stars are ejected from the cluster with a high velocity due to their initial kick. Once far enough away, the code seems to treat pairs of such neutron stars as binaries and the three-body interaction between these and the rest of the cluster eventually reduces the timestep to zero and halts the simulation. Removing stars at a large radius from the cluster eliminates this problem.

3. Initial Conditions

We perform five simulations: a single generation model with a Salpeter IMF (SP), a single generation model with a D’Antona and Caloi top-heavy IMF (DC), and three two-generation models with a D’Antona and Caloi IMF for the first generation and a Salpeter IMF for the second generation (Ca, Cb, and Cc). In all cases we follow Hurley et al. (2005) and use Plummer models for our initial conditions. In the two-generation models we allow the first generation to evolve for ~ 200 Myr before adding the second generation according to a Salpeter IMF. In all cases the initial virial radius is the length unit and is set to 5.0 pc. The mass unit for each simulation is the total mass of the simulated cluster. The energy and time units are defined by starting all simulations in virial equilibrium. Parameters for these simulations are given in Table 1. The number of particles used in these simulations is a compromise between achieving an accurate number of particles and our hardware limitations. Fukushige & Heggie (1995) have explored the behavior of clusters with different mass functions and find that there is little difference between simulations carried out with 8192 and 16384 particles. Practically, we find that ~ 12000 particles is the maximum number for which we can achieve a reasonable wall-clock time and since we are in the middle of the 8000-16000 particle range, we do not expect our results to scale to strongly with particle number. All clusters are simulated in isolation in order to keep our parameter space small and to eliminate effects that are not due to the addition of the second generation. We must, however, introduce a stripping radius for the reasons discussed above. We find that by stripping at 100 initial virial radii we eliminate the problematic fast-moving neutron stars while removing few other stars from the simulations.

4. Results

We consider results for the dynamical and final stellar populations of our simulations separately.

4.1. Dynamics

We present the initial half-mass relaxation times and some of the final physical data for our systems in Table 2. Each cluster has lost a significant portion of its initial mass. Few particles are removed from the simulations and this mass loss is due to stellar evolution rather than loss of stars from the cluster. This mass-loss is particularly pronounced in DC with its extreme initial enhancement of high-mass stars and is also a major factor in the two-generation clusters with their top-heavy first-generation IMFs. We find the initial half-mass relaxation times of the two-generation clusters to be somewhat smaller than that of the single generation Salpeter IMF while the half-mass relaxation time of the single-generation cluster with the D’Antona and Caloi IMF is much shorter than any of the other cases. Since each cluster has the same initial virial radius and thus the same initial physical concentration, the differences are due to the initial total mass increasing from SP through the two-generation clusters to DC. It is worth noting that the combined clusters undergo a sufficient number of relaxation times to allow the possibility of core collapse by the end of our simulations.

In Figure 3 we present a comparison of the Lagrangian radii for the runs SP, DC and Ca (Cb and Cc are similar to Ca). The evolution of the Lagrangian radii for SP is slightly different from Ca and DC. In DC and Ca the Lagrangian radii grow quickly at first and then flatten significantly, with the 75% radius still growing slowly and the 50% and 10% flattening (and even contracting in the case of the 10% and 50% massive radii of Ca). By contrast the early growth period is much less evident in SP and all radii continue to grow slowly (with the 10% radius flattening at the end). The difference is due to the high-mass stars in DC and the first generation of Ca. These high-mass stars evolve quickly and consequently lose a great deal of mass over a short timescale (the first generation of Ca loses $\sim 30\%$ of its mass in 200 Myr). This mass-loss leads to a rapid reduction in cluster potential, causing rapid cluster expansion and a consequent increase in the Lagrangian radii. Once the high-mass stars evolve away, mass-loss becomes dominated by low-mass stars which evolve much more slowly leading to a much reduced mass-loss rate and a subsequent flattening of the Lagrangian radii. By contrast SP is always dominated by low-mass stars and experiences slow, constant mass-loss throughout its life, consequently displaying slow, constant expansion.

We compare the Lagrangian radii of the most massive 10% of stars (cutoff masses given

in Table 2) to the Lagrangian radii for the entire system in Figure 3. We note that there is a wide separation between the massive and overall Lagrangian radii in SP and Ca while for much of the life of DC the massive and overall Lagrangian radii are similar. That the massive Lagrangian radii are smaller indicates the high-mass stars are more centrally concentrated than the low-mass ones. This is a manifestation of mass segregation which is a natural consequence of equipartition of energy in phase space and is expected in all N-body systems with a range in initial masses (Binney & Tremaine 1987). The smaller spread between the overall and massive population in DC seems to indicate that mass segregation is less advanced in this simulation than in SP and Ca. This is somewhat unexpected since for an N-body system the timescale for mass segregation is on the order of the two-body relaxation time (Binney & Tremaine 1987). Since DC has the shortest half-mass relaxation time of our simulations we would expect mass segregation would be the most advanced in this model. We postulate that the larger spread and higher overall mass in the IMF of DC (Figure 1) both renders the overall statistics of this simulation less sensitive to the effects of a few very high-mass stars in the central regions and produces a more smooth transition between the low-mass halo and the high-mass core. Both of these processes could bring the overall and massive Lagrangian radii closer together without actually indicating a reduction in mass-segregation. It is worth noting that mass segregation indeed does become more pronounced in DC after 5-10 T_{RH} after the most massive stars have evolved away and the mass function has become more peaked. SP and Ca both exhibit extensive mass segregation based on the Lagrangian radii with SP exhibiting a slightly larger discrepancy between the massive and overall radii than Ca. Again Ca has a shorter two-body relaxation timescale than SP and we invoke the same idea as in DC to explain this effect. Thus, since both SP and Ca exhibit a similar size at each overall Lagrangian radius, we do not expect two-generation clusters to be reliably distinguishable from their single-generation counterparts by observations of overall size or mass segregation.

In Figure 4 we consider the final density profiles of all simulated clusters. Note that the 75% Lagrangian radius is at $\log r/r_{vir} \approx 1$ and the profile is noisy outside this region due to low-number statistics. The density profiles are remarkably similar with all clearly exhibiting an exponential halo and a flatter core. Ca and Cb are almost indistinguishable from SP except at the very center. DC is slightly less dense than the others but has essentially the same profile. The only simulation which displays a significant deviation is Cc with a steeper core profile than the other simulations. Cc differs from the other two-generation clusters in other ways and will be discussed in more detail in § 4.1.1.

In Figure 5 we consider the radial velocity dispersion profile for all simulated clusters. Again the 75% Lagrangian radius is at $\log r/r_{vir} \approx 1$ and statistics beyond this are point unreliable due to low numbers. We note that the cores of Ca and Cb are slightly more

distinct than SP and DC and that all profiles are vertically shifted compared to each other. These variations are as large between the two-generation clusters themselves as between the two-generation and single-generation clusters and they are merely simulation-to-simulation variations. The peaks in Ca and Cb are caused by high-velocity single stars and are a product of low-number statistics. The largest outlier is again Cc and we now turn to a discussion of this simulation.

4.1.1. *Simulation Cc*

We consider core densities as a function of time for all simulations in Figure 6. Unlike the other simulations, Cc exhibits a clear peak in core density at approximately $15 T_{RH}$ (≈ 11.5 Gyr), corresponding nicely to the steeper density profile in the core region in Figure 4. We tentatively propose that Cc has experienced a core-collapse event at $15 T_{RH}$. If correct, this is an interesting result and tells us that the dynamics of two-generation clusters are similar to those of their single-generation counterparts in yet another way. That only one simulation would experience core collapse at a specific time is not surprising since the onset of core collapse is associated with individual escapers and hard binaries, the specifics of which vary between simulations. We caution, however, that with only 12000 particles such a peak could be caused by a few massive stars in the core region rather than a full core-collapse event. We also note that the kinetic energy of escapers in a core-collapsed cluster should be systematically higher than in a non-core-collapsed cluster due to binary scattering from the core. This is not the case for Cc (Table 2). Further simulations with more particles are needed to fully pin down the core-collapse behaviour of two-generation clusters.

4.2. Stellar Population

Finally, we consider the stellar populations of the clusters. In Figure 7 we present, as histograms, the final mass functions for SP, DC and Ca. In the case of SP there has been very little evolution in the mass function. The number of $0.7 - 1M_{\odot}$ stars has been slightly enhanced due to the evolution of high-mass stars into white dwarfs but the stellar population is still dominated by low-mass main sequence stars (Table 3). By contrast both DC and Ca are very strongly peaked at $0.7 - 1M_{\odot}$. This peak is composed mainly of C-O white dwarfs with intermediate-mass progenitors and which make up a much greater fraction of the population than they do in SP. Indeed DC is dominated by such compact remnants (Table 3). The strong double peak in the mass function of Ca is also to be noted as it resembles the combination of the final mass function for SP and DC, as would be expected

for a cluster formed from a combination of two such IMFs. These mass functions are all quite different and indeed all three types of clusters should be distinguishable by obtaining accurate white dwarf to main sequence star number ratios. Recent observations of NGC 6752 (Ferraro et al. 2003) show an anomalously high mass-to-light ratio in the core which might be indicative of a large population of low-luminosity, compact objects such as old white dwarfs. A early, massive generation could be one way of producing such an excess although much more study is needed before we would seriously propose this scenario as an option in particular cases.

5. Conclusions

We have considered the plausibility of a two-generation formation scenario for galactic globular clusters from the standpoint of dynamics and to a lesser extent stellar populations. Based on our simulations we expect two-generation clusters to be long-lived objects that at the current age of the galactic globular cluster population are very dynamically similar to their single-generation counterparts. We tentatively propose that two-generation clusters can undergo core collapse at a similar time to the single generation clusters, although more investigation is needed on this front. We expect two-generation clusters with top-heavy IMF first-generations to have different stellar populations and specifically we predict that two-generation clusters with a top-heavy IMF would be strongly enhanced in white dwarf stars. Clusters observed to have such an enhancement would be candidates for the D’Antona and Caloi two-generation formation scenario.

There are two areas in particular that could use further expansion. The first is the treatment of the ejecta in the initial generation. In particular a more complete treatment of the gas and a full exploration of different star formation efficiencies would be useful in order to make predictions about young clusters. In particular it has been shown (Bastian & Goodwin 2006) that rapid loss of gas from a young cluster can leave the remaining stellar component out of equilibrium. The loss of the non-star-forming fraction of the ejecta from the first generation could have a similar result on the initial state of a two generation cluster and deserves exploration. The second area is to perform further simulations to pin down exactly when a two-generation cluster will experience core collapse.

Based on our simple simulations, we find that two-generation clusters are plausible on the basis of dynamics and could form a fraction of the population of galactic globular clusters. Interestingly Karakas (2006) show that AGB stars may not be capable of producing sufficient helium enhancement to produce the BHB of NGC 2808 without violating other constraints (most importantly $C + N + O \sim const.$). Thus, although we find two-generation clusters to

be a dynamical possibility, the application of the two-generation scenario to the motivating example cluster remains in doubt.

A. Appendix A

The top-heavy IMF from D’Antona & Caloi (2004) is not included in the standard set of Starlab IMF prescriptions and we have encoded it ourselves. First we fix the constants c_1 and c_2 by the number of RHB stars in NGC 2808, the specific choice of M_B , α and β and the criterion $c_1 M_B^{-(1+\alpha)} = c_2 M_B^{-(1+\beta)}$. This yields:

$$c_1 = \left. \frac{dN}{dM} \right|_{M_{RHB}} \times M_{RHB}^{-(1+\alpha)} \quad c_2 = c_1 M_B^{(\beta-\alpha)}$$

We can then calculate the number of stars in the α and β regimes:

$$N_\alpha = c_1 \frac{M_B^{-\alpha} - M_l^{-\alpha}}{-\alpha} \quad N_\beta = c_2 \frac{M_{up}^{-\beta} - M_B^{-\beta}}{-\beta}$$

The mass for an individual node is then generated using the prescription:

$$M = \begin{cases} M_l [(((\frac{M_B}{M_l})^{-\alpha} - 1)P_m + 1)^\alpha] & P_{mr} \leq \frac{N_\alpha}{N} \\ M_B [(((\frac{M_{up}}{M_B})^{-\beta} - 1)P_m + 1)^\beta] & P_{mr} > \frac{N_\alpha}{N} \end{cases}$$

where P_{mr} and P_m are random numbers between zero and one which determine respectively the mass regime a star will be in (α or β) and what its mass in that regime will be. This mass-function is defined entirely by the choice of α , β and M_B and produces the needed enhancement in high-mass stars.

REFERENCES

- Alcaino, G. 1969, ApJ, 156, 853
- Bastian, N., & Goodwin, S. P. 2006, MNRAS, 369, L9
- Bedin, L. R., Piotto, G., Zoccali, M., Stetson, P. B., Savaiane, I., Cassisi, S., & Bono, G. 2000, A&A, 363, 159
- Binney, J., & Tremain, S. 1987, Princeton University Press
- Catelan, M., & de Freitas Pacheco J. A. 1995, A&A, 297, 345

- D’Antona, F., Bellazzini, M., Caloi, V., Pecci, F. F., Galletti, S., & Rood, R. T. 2005, *ApJ*, 631, 868
- D’Antona, F., & Caloi, V. 2004, *ApJ*, 611, 871
- D’Antona, F., Caloi, V., Montalbán, J., Ventura, P., & Gratton, R. 2002, *A&A*, 395, 69
- Eggleton, P. P., Tout, C. A., Fitchett, M. J. 1989, *ApJ*, 347, 998
- Farouki, R. T., & Salpeter, E. E. 1982, *ApJ*, 253, 512
- Ferraro, F. R., Possenti, A., Sabbi, E., Lagani, P., Rood, R. T., D’Amico, N., & Origlia, L. 2003, *ApJ*, 595, 179
- Fukushige, T. & Heggie, D. C. 1995, *MNRAS*, 276, 206
- Fukushige, T., Makino, J., & Kawai, A. 2005, *PASJ*, 57, 1009
- Gnedin, O. Y., Zhao, H., Pringle, J. E., Fall, S. M., Livio, M., & Meylan, G. 2002, *ApJ*, 568, L23
- Goodwin, S. P. 1997, *MNRAS*, 284, 785
- Gratton, R., Sneden, C., & Carretta, G. 2004, *ARA&A*, 42, 385
- Hansen, B. M. S., Brewer, J., Gahlman, G. G., Gibson, B. K., Ibata, R., Limongi, M., Rich, R. M., Richer, H. B., Shara, M. M., & Stetson, P. B. 2002, *ApJ*, 574, L155
- Harris, W. E. 1974, *ApJ*, 192, L161
- Harris, W. E. 1996, *AJ*, 112, 1487
- Hurley, J. R., Pols, O. R., Aarseth, S. J., & Tout, C. A. 2005, *MNRAS*, 363, 293
- Karakas, A., Fenner, Y., Sills, A., Campbell, S. W., & Lattanzio, J. C. 2006, *MmSAIt*, 77, 858
- Kraft, R. P., Sneden, C., Langer, G. E., & Prosser, C. F. 1992, 104, 645
- Kroupa, P. 2001, *MNRAS*, 322, 231
- Kroupa, P. 2002, *Science*, 295, 82
- Lada, C. J., & Lada, E. A. 2003, *ARA&A*, 41, 57
- Meissner, F., & Weiss, A. 2006, *A&A*, 456, 1085

- Piotto, G., Villanova, S., Bedin, L. R. Gratton, R., Cassisi, S., Momany, Y., Recio-Blanco, A., Lucatello, S., Anderson, J., King, I. R., Pietrinferni, A., & Carraro, G. 2005, *ApJ*, 621, 777
- McMillan, S. L. W. 1986, *ApJ*, 307, 126
- Portegies Zwart, S. F., McMillan, S. L. W., Hut, P., & Makino, J. 2001, *MNRAS*, 321, 199
- Pryor, C., and Meylan, G. 1993, *ASP Conf. Ser.* 50, 357-371
- Salpeter, E. E. 1955, *ApJ*, 121, 161
- Spitzer, L. 1987, *Dynamical Evolution of Globular Clusters*, Princeton University Press

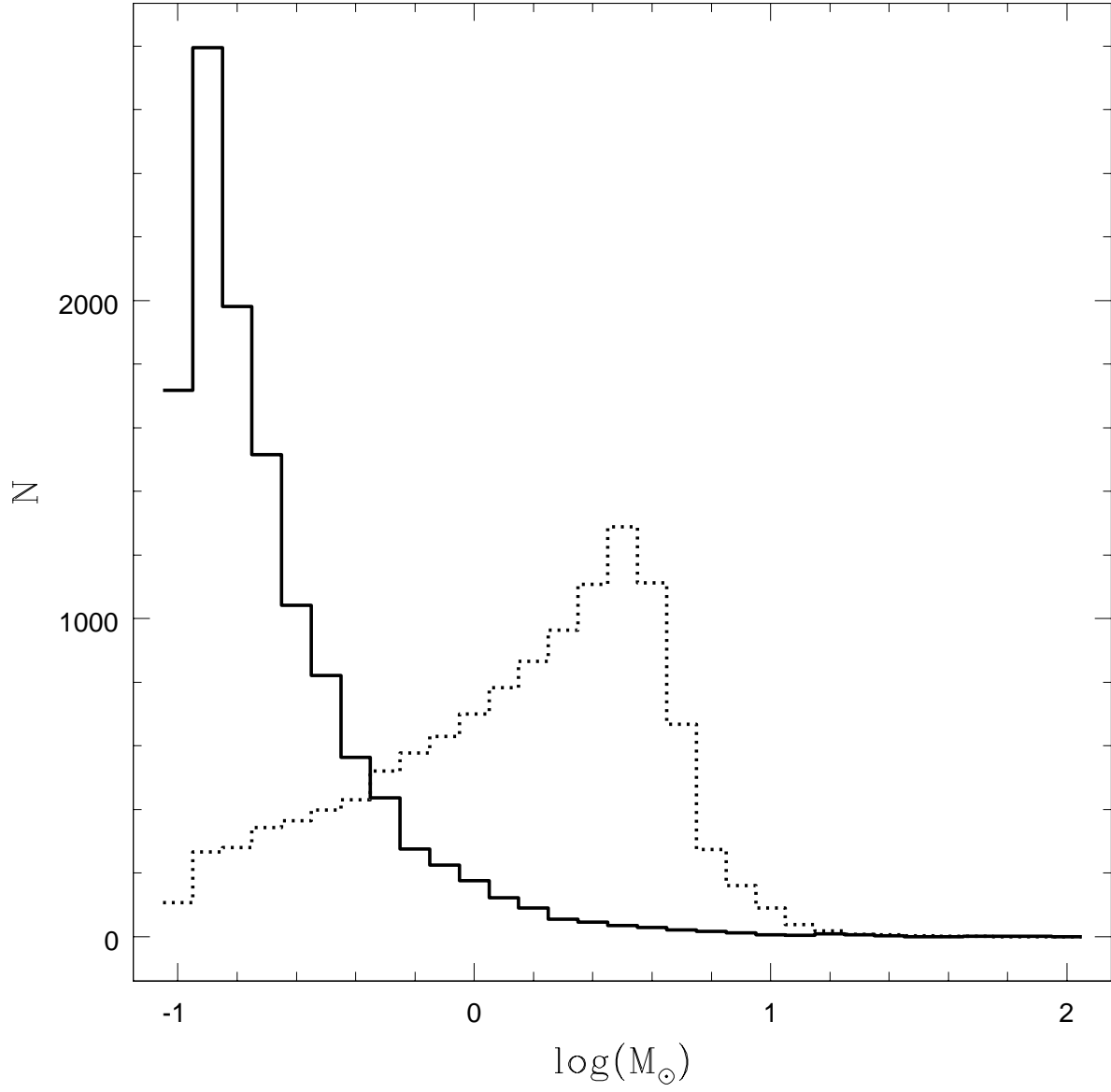


Fig. 1.— A D’Antona and Caloi IMF (dotted line) prepared by our new Starlab algorithm compared with a Salpeter IMF prepared using one of the standard Starlab algorithms (solid line).

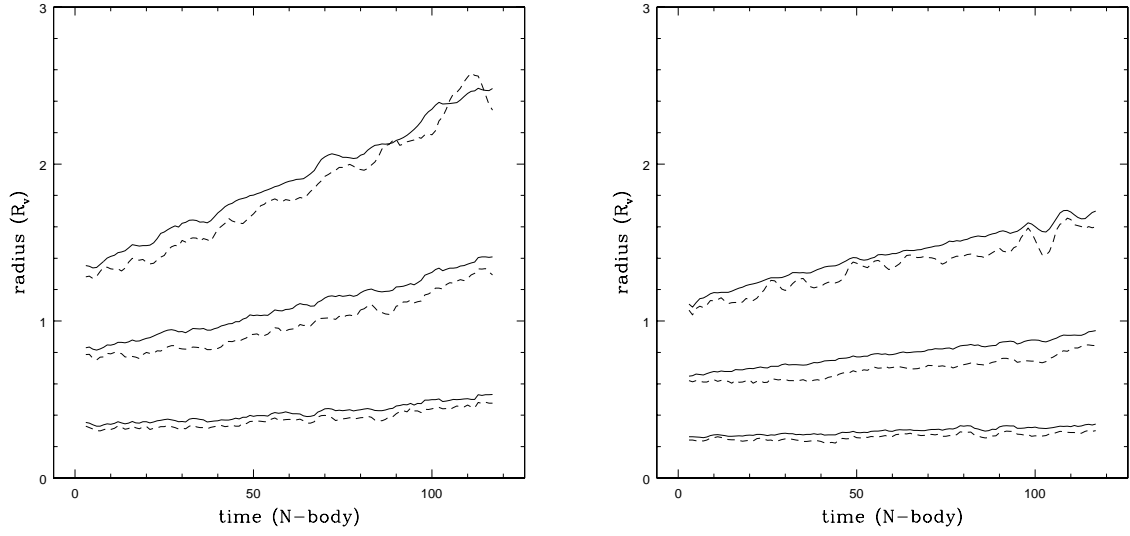


Fig. 2.— On the left are shown the Lagrangian radii for a cluster with a top-heavy IMF evolving for 200 Myr. On the right are the Lagrangian radii for the same cluster evolving in a Plummer potential with a static mass equal to the mass lost to stellar evolution over the 200 Myr life of the cluster. From bottom are the 10%, 50% and 75% Lagrangian radii. Solid indicates the entire system, dotted indicates the most massive 10% of stars.

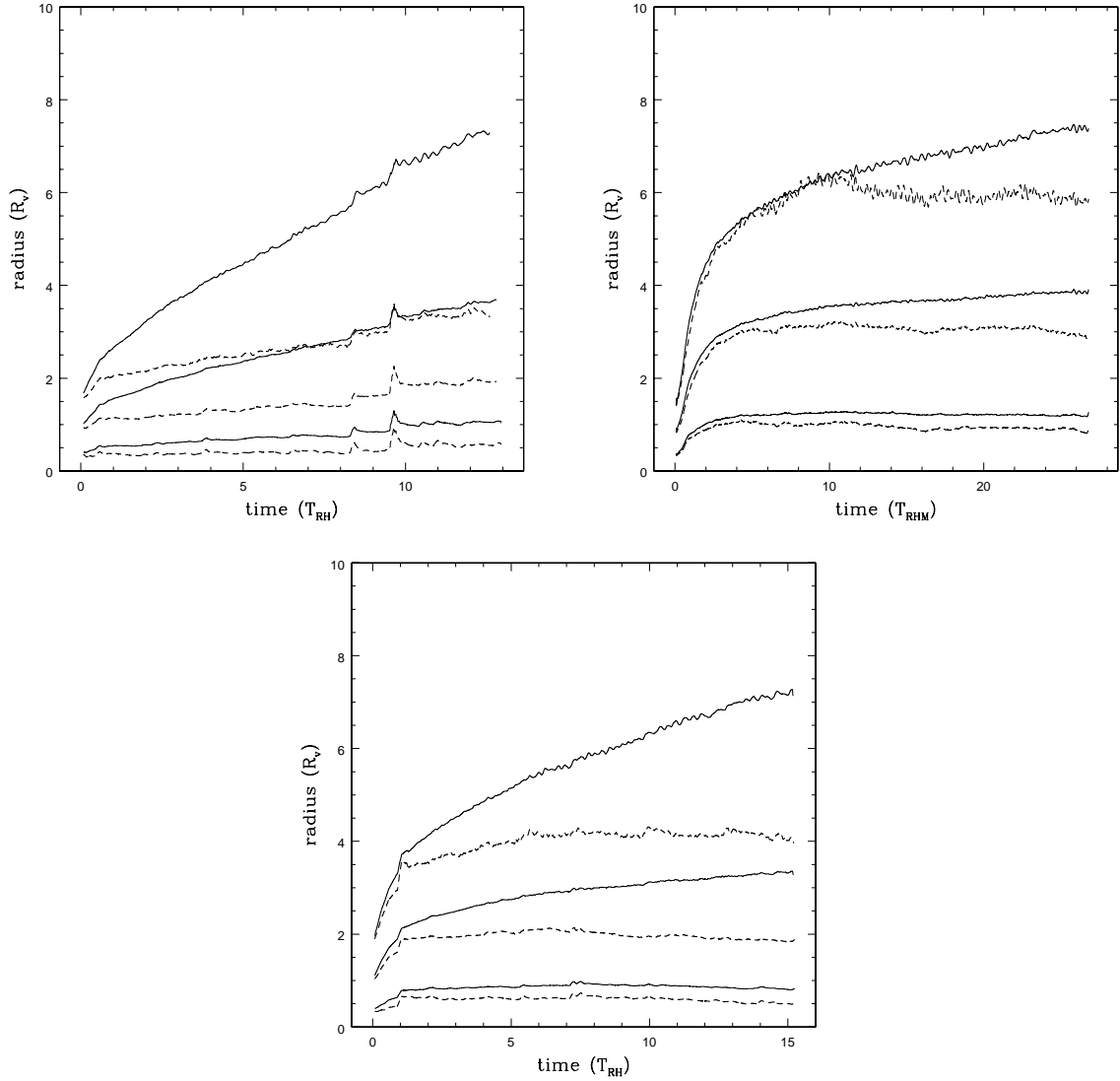


Fig. 3.— The Lagrangian radii for a Salpeter IMF (top left), a D’Antona and Caloi IMF (top right) and a D’Antona and Caloi IMF with a second generation added according to a Salpeter IMF (bottom). From bottom to top in each graph are the 10%, 50% and 75% Lagrangian radii. Solid is for all stars, dotted for the most massive 10% of stars. The spike just before $10 T_{RH}$ in SP is created by the ejection of a massive binary from the cluster core.

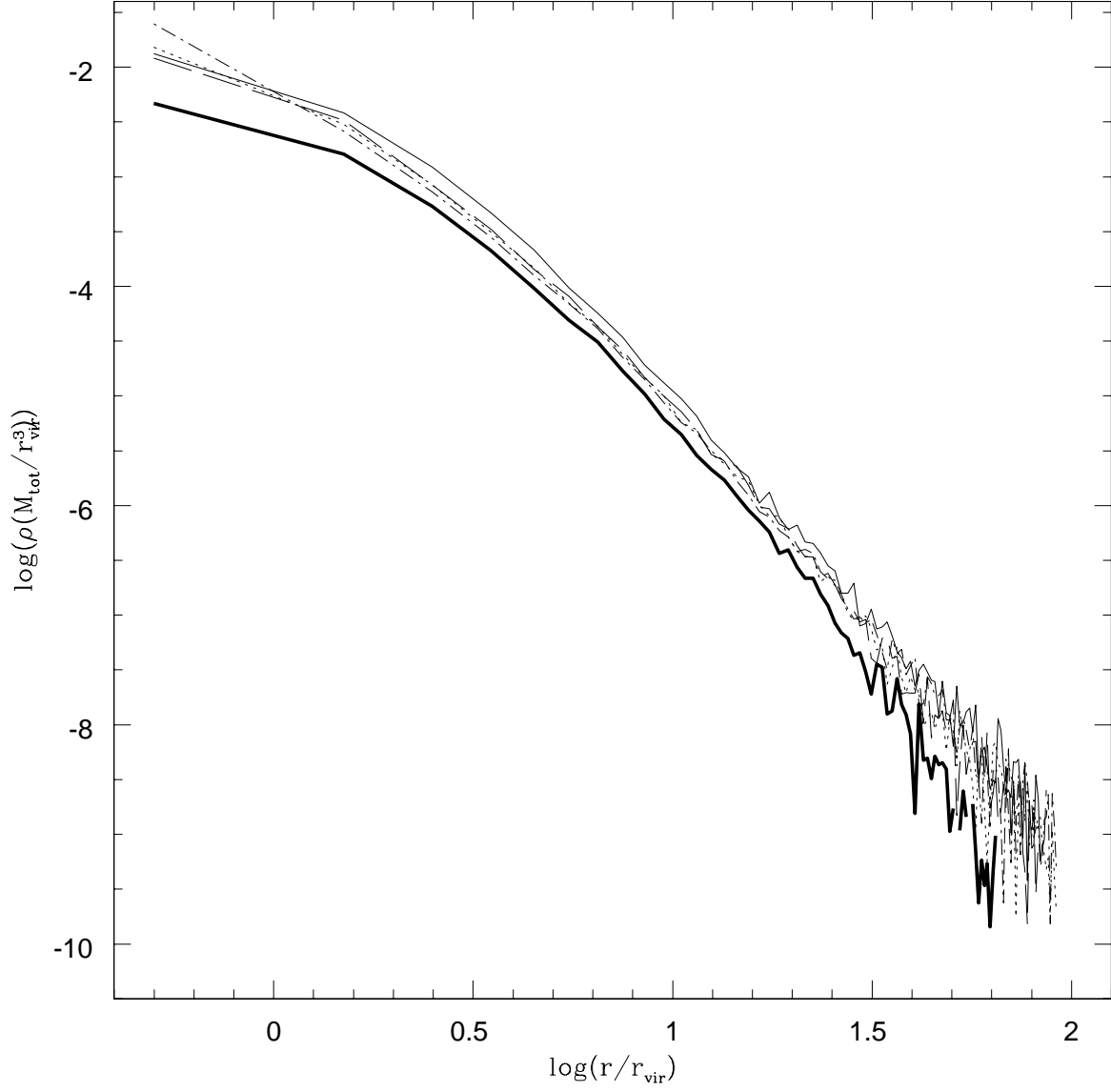


Fig. 4.— The radial density profiles of the simulated clusters. Thin solid is SP, thick solid is DC, dotted is Ca, broken is Cb and dot-dashed is Cc. Profiles are taken to the stripping radius (100 initial R_{vir}).

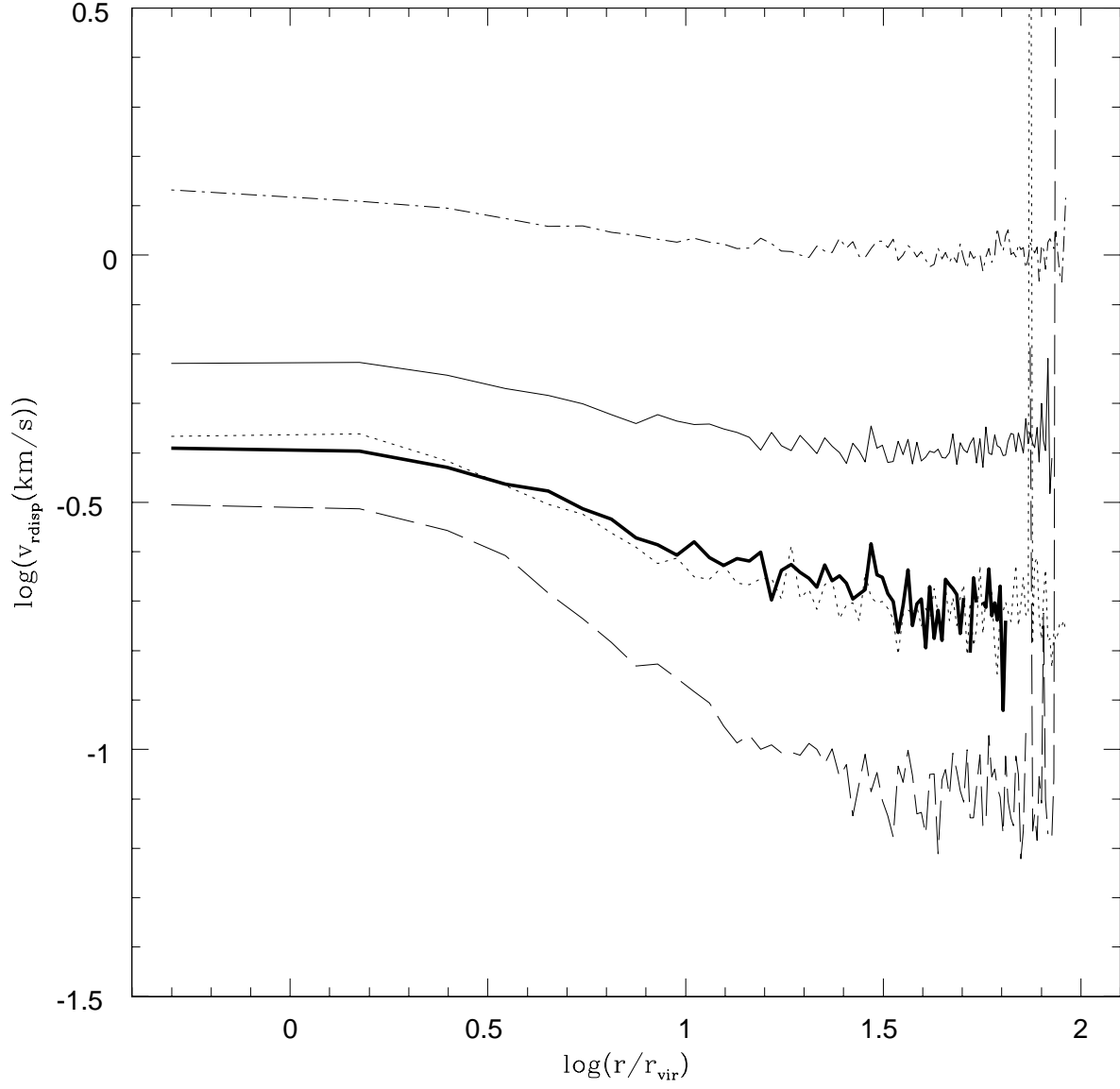


Fig. 5.— Profiles of the radial velocity dispersion for the simulated clusters. Thin solid is SP, thick solid is DC, dotted is Ca, broken is Cb and dot-dashed is Cc. Profiles are taken to the stripping radius (100 initial R_{vir}).

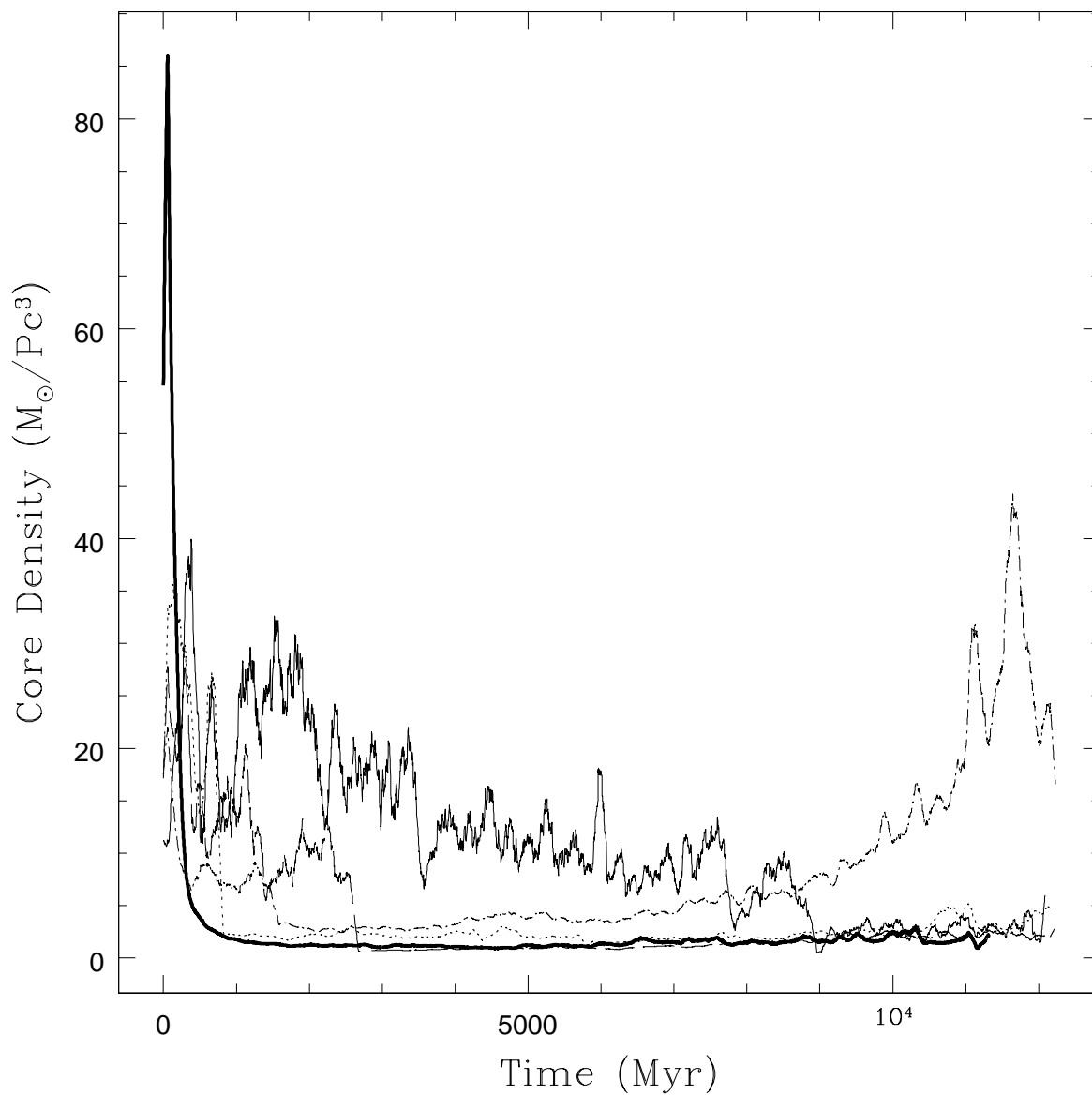


Fig. 6.— Core densities for the simulated clusters as a function of time. Thin solid is SP, thick solid is DC, dotted is Ca, broken is Cb and dot-dashed is Cc. Time is physical so that all simulations can appear on the same graph.

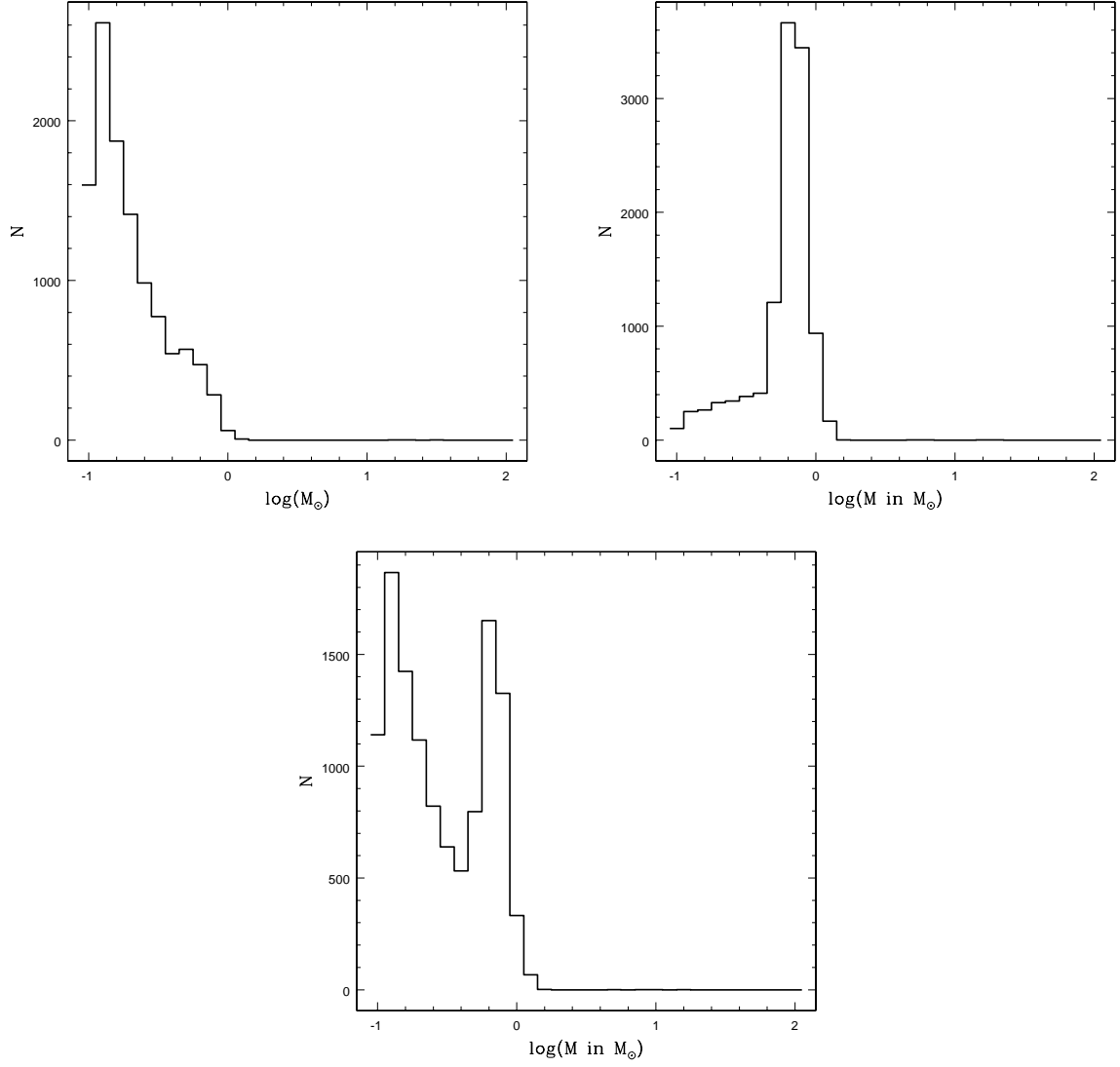


Fig. 7.— Histograms displaying the final mass function for the clusters SP (top left), DC (top right) and Ca (bottom).

Simulation Parameters				
Run ID	1 st gen		2 nd gen	
	N	$M_{tot}(M_{\odot})$	N	$M_{tot}(M_{\odot})$
SP	12000	4275	-	-
DC	12000	26312	-	-
Ca	4096	9093	8350	3132
Cb	4096	9053	8400	3061
Cc	4096	9032	8300	2982

Table 1: The parameters used to initialize our eight simulations. ID identifies the run. The total particle number and total mass are then given for the first and second generation respectively (the mass of the second generation matches the mass lost in the first).

Final Physical Parameters							
ID	N_f	$M_f(M_{\odot})$	$T_{RH}(\text{Myr})$	Final Age(Gyr)	$M_{10\%in}(M_{\odot})$	$M_{10\%fin}(M_{\odot})$	K_{esc} (N-body)
SP	11189	2684	930.2	12.1	0.5407	0.5147	7.376E-2
DC	11507	7308	413.9	11.3	4.537	0.8864	2.307E-4
Ca	11718	4336	799.8	12.2	2.053	0.7689	7.650E-3
Cb	11842	4370	736.3	12.4	2.072	0.7693	1.764E-3
Cc	11661	4359	738.3	12.4	2.120	0.7744	1.831E-3

Table 2: Column (1) gives the run ID, (2) is the final particle number, (3) is the final mass of the system, (4) is the initial half-mass relaxation time, (5) is the final age of the cluster, (6) and (7) respectively the initial and final cut-off masses for stars to be included in the calculation of the massive Lagrangian radii and (8) is the kinetic energy of all stars with a square of velocity greater than four times the RMS velocity.

Final Stellar Populations					
Type	SP	DC	Ca	Cb	Cc
Main Sequence	10688	3886	8736	8844	8587
White Dwarfs	461	7453	2896	2903	2997
Neutron Stars	0	30	15	16	11
Black Holes	2	4	3	2	1
Other	38	134	68	77	65

Table 3: The final stellar populations for each simulation. “Other” includes subgiant, Hertzsprung gap, horizontal branch etc.